Erschienen in: IEEE Journal of Photovoltaics ; 10 (2020), 1. - S. 85-93
https://dx.doi.org/10.1109/JPHOTOV.2019.2954768

Influencing Light and Elevated Temperature Induced Degradation and Surface-Related Degradation Kinetics in Float-Zone Silicon by Varying the Initial Sample State

Benjamin Hammann, Josh Engelhardt, David Sperber, Axel Herguth, and Giso Hahn

***Abstract*—Light and elevated temperature induced degradation (LeTID) kinetics in float-zone silicon are investigated by varying the initial sample state, composed of different base material, base doping, SiN_x:H films, and subsequent firing, and/or annealing steps. The approach of deliberately changing the initial sample state is shown to allow for specific studies of influences of LeTID kinetics. Bulk- and surface-related degradations are examined separately and the influence on the kinetics of bulk- and surface-related degradation is illustrated by a four-state and three-state model, respectively. In case of bulk-related degradation, an increase in defect density because of the firing step is shown, whereas the annealing step has an inverse effect. Both temperature steps—individually and combined—influence the transition rates of bulk-related degradation and regeneration by presumably changing the distribution of a defect precursor. For surface-related degradation, the firing step reduces the transition rate from the initial to the degraded state. In addition, the influence of a comparably humid atmosphere and the absence of UV light are found to be negligible.**

***Index Terms*—Bulk-related degradation (BRD), crystalline silicon, defect density, float zone (FZ), light and elevated temperature induced degradation (LeTID), surface-related degradation (SRD).**

I. Introduction

LIGHT and elevated temperature induced degradation (LeTID) is a degradation phenomenon first found especially in mc-Si in 2012 [1]. Recently, a similar or the same phenomenon was discovered in Cz-Si [2], [3] and float-zone (FZ) Si [4], [5]. Compared with other degradation effects like boron-oxygen-related (BO) degradation [6], higher treatment temperatures >50 °C are needed to investigate the effect on experimentally viable time scales [1], [7]. Besides LeTID, which is a bulk-related degradation (BRD), a second degradation phenomenon is visible and can be identified as a surface-related degradation (SRD) [8]. In this article, the initial sample state is varied to investigate its influence on LeTID and SRD kinetics. The initial sample state is composed of the Si base material, the SiN_x:H deposition, and additional firing and/or annealing steps. Their respective influence is investigated individually via separating bulk and surface defect densities. The results shown here confirm recent publications as well as reveal features concerning LeTID in FZ-Si for the first time.

By changing the initial sample state, it is possible to investigate the influence on the kinetics of both BRD and SRD more precisely. A nonfired sample with BRD is used to show the influence of firing and annealing steps. The samples are subjected to either one of the temperature steps or a combination of both, and their respective influence on the density of recombination active defects and the transition rates are investigated. The combination of both temperature steps leads to different kinetics, depending on the order of temperature steps as well as the annealing duration. Whereas all samples are susceptible to SRD, BRD kinetics are influenced in a different way than SRD kinetics. In addition, the influence of humidity and UV light on SRD is investigated under realistic conditions.

This work was supported by the German Federal Ministry for Economic Affairs and Energy under Contracts 0324226A and 0324001. *(Corresponding author: Benjamin Hammann.)*

The authors are with the Department of Physics, University of Konstanz, 78457 Konstanz, Germany (e-mail: benjamin.hammann@uni-konstanz.de; josh.engelhardt@uni-konstanz.de; david.sperber@uni-konstanz.de; axel.herguth@uni-konstanz.de; giso.hahn@uni-konstanz.de).

II. Theoretical Background

Fig. 1 schematically depicts both BRD and SRD, their respective regeneration [9], and the models that are used in this article. The model for BRD consists of a defect precursor state A, the recombination-active state B, and a regenerated state C. It is based on the four-state model by Fung *et al.* [10] (compare Fig. 1), which has an additional reservoir state R that is not necessary for the findings of this article. The defect transition between two states is described via transition rates k_{ij}, where i is the initial and j the final state. In the following, this model is used to investigate the kinetics of samples with different temperature steps. For SRD, a three-state model is used with an initial, a degraded, and a regenerated state. Although the regeneration of SRD is not explicitly observed in this article, previous works [9], [11] allow to expect that by using longer measurement times, it would have led to the occurrence of regeneration of SRD. Therefore, the focus for SRD lies on the degradation and the transition between the two first states with a transition rate k_{SRD}.

Konstanzer Online-Publikations-System (KOPS)
URL: http://nbn-resolving.de/urn:nbn:de:bsz:352-2-aas0xbv6bh1q8

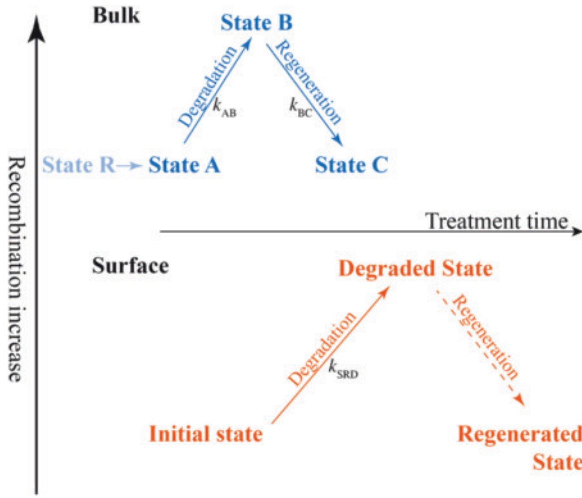

Fig. 1. Schematic representation of the four-state model for BRD and three-state model for SRD and the influence of these degradations on recombination.

The root cause of both BRD and SRD is yet unknown. Although hydrogen is a likely candidate to impact BRD [12], [13], it is still under discussion whether the defect is formed in combination with additional species. SRD, in turn, is a degradation of chemical passivation quality in case of, e.g., SiN_x:H passivation and of field effect passivation quality in case of, e.g., AlO_x/SiN_x:H passivated samples [11]. SRD is likely linked to hydrogen [8], although again its cause is also not yet known. Both degradation phenomena seem to be linked to the firing step as a high-temperature treatment process step. With higher temperatures, a stronger degradation occurs [13], [14], although recent results [15] with unfired samples question the theory that the firing step enhances BRD.

Since recombination is the limiting factor, the effective “excess” charge carrier lifetime τ_{eff} allows the analysis of recombination mechanisms. Using τ_{eff}, one can calculate the lifetime-equivalent defect density ΔN_{leq} [16] as the difference of inverse effective excess charge carrier lifetimes. Per sample, one reference value $\tau_{\text{eff}}(t_0)$ is chosen in order to investigate the changes with respect to the lifetime reference point. The lifetime-equivalent defect density corresponds to a change in density of a single defect described by the Shockley–Read–Hall theory while having no changes to surface passivation [16]

$$\Delta N_{\text{leq}} = \frac{1}{\tau_{\text{eff}}(t)} - \frac{1}{\tau_{\text{eff}}(t_0)} \propto \Delta N_{\text{SRH}}. \tag{1}$$

As previously mentioned, in FZ-Si BRD and SRD occur. Therefore, it is necessary to separate bulk from surface-related effects. This is done by analyzing the saturation current density at the surface J_{0s} according to [17] as it was demonstrated already in [8]. With J_{0s}, it is possible to calculate a lifetime-equivalent defect density at the surface $\Delta N_{\text{leq},s}$ according to [16]

$$\Delta N_{\text{leq},s} = \frac{2(p_0 + \Delta n)}{qwn_i^2} \cdot (J_{0s}(t) - J_{0s}(t_0)) \tag{2}$$

with p_0 being the equilibrium density of holes, Δn the charge carrier injection, q the elementary charge, w the thickness, and n_i the intrinsic charge carrier density. SRD is described via $\Delta N_{\text{leq},s}$, whereas for BRD $\Delta N_{\text{leq},b}$ is used. The latter can be calculated by subtracting the surface-related defect density from total ΔN_{leq}

$$\Delta N_{\text{leq},b} = \Delta N_{\text{leq}} - \Delta N_{\text{leq},s}. \tag{3}$$

$\Delta N_{\text{leq},b}$ can be directly related to the density of defects converting to the recombination-active state of the four-state model $\Delta N_{\text{leq},b} \propto \Delta N_B$ and is used to describe changes in the BRD kinetics. In the same manner, $\Delta N_{\text{leq},s}$ is used to describe the changes of the defect density of the degraded state and therefore the SRD kinetics. Since both defect compositions are not yet fully understood, the investigation of influences on their respective kinetics can provide further information about the defect structure.

TABLE I
DIFFERENT BASE MATERIALS WITH THEIR RESPECTIVE REFERENCE USED IN THIS ARTICLE

Doping type	Base doping / Ωcm (manufacterer’s data)	Referred to as
p-type (B-doped)	1.7 (1.7 – 2.3)	2p
p-type (B-doped)	200 (170 -230)	200p
n-type (P-doped)	2.3 (1-5)	3n
n-type (P-doped)	200 (160-240)	200n

III. EXPERIMENTAL DETAILS

As base material, 250-μm-thick FZ silicon substrates supplied by Siltronic AG were used with variations shown in Table I.

The FZ-Si wafers did not receive a chemical treatment after removal from the shipment box and therefore feature a 2–3 nm thick, wet-chemically grown silicon oxide layer (SiO_x). The FZ wafers were cut into pieces of approximately 5 × 5 cm^2 and received a consecutive deposition of hydrogen-rich silicon nitride (SiN_x:H) on both sides. Two different tools were used for deposition, both using plasma-enhanced chemical vapor deposition techniques. Both techniques result in 70 nm thick SiN_x:H with a refractive index $n_{633\text{nm}} \sim 2$. Most of the samples were processed in a PlasmalabSystem100 from Oxford Instruments (deposited SiN_x:H further referred to as SiN-1). The deposition process takes ~8 min at 400–450 °C per side. This is faster than the second tool, an industrial setup from Centrotherm International AG, in which the deposition takes per side around 40 min at 400–450 °C (deposited SiN_x:H further referred to as SiN-2). Evaluations of fourier-transform infrared spectroscopy (FTIR) measurements after deposition (not shown here) resulted in an approximately 33% higher peak of the N–H binding at 3350 cm^{-1} (see, e.g., [18]) in SiN-2 suggesting a higher H density in this specific SiN_x:H.

As depicted in the process chart (see Fig. 2), the samples may receive a firing or annealing step after deposition. For firing, a belt furnace c.FIRE from Centrotherm International AG is used with the firing profile optimized in such a way that the maximum sample temperature equals 800 ± 15 °C. A tube furnace with a set temperature of 450 °C and a sample temperature of approximately 400 °C is used for the annealing process. The annealing step takes place in a N_2 atmosphere. The duration of this annealing step is either 5 or 30 min. In order to keep the processing procedure as simple as possible,

Fig. 2. Schematic overview of the investigated samples and their respective initial state. Group I is used to investigate the influence of firing and annealing steps on the kinetics of LeTID, whereas samples of Group II are used to study the influence of different base materials and SiN$_x$:H depositions.

further temperature treatments like preoxidation or $POCl_3$ diffusion have been omitted. Investigations from Sperber *et al.* [19] show that despite these treatments BRD and SRD occur. The re-evaluation of these experiments in [20] shows that the samples show different degradation behavior when subjected to different high temperature steps. By excluding additional high temperature treatments, the sample is only influenced by its base material, the SiN$_x$:H deposition, and subsequent temperature steps thus defining the individual initial state of each sample and making the influence of each respective part easily accessible.

Samples are then placed in a SunEvent SUN/600/S climate chamber from Weiss Umwelttechnik. The samples are treated in the chamber at 800 $\pm$ 20 W/m^2, with a sun-like spectrum according to CIE No. 85, 100 $\pm$ 2 °C and 50% relative humidity (RH), although for a specific study humidity is varied where the humidity is depicted separately. Injection-dependent effective lifetime $\tau_{\text{eff}}(\Delta n)$ is measured at different treatment times using a WCT-120 lifetime tester from Sinton Instruments.

For the calculation of $\Delta N_{\text{leq}(,s,b)}$, τ_{eff} is chosen such that it is as close as possible to the crossover point of FeB-pair dissociation [21]. The best injection level to neglect the influence of FeB-pair dissociation would be $2 \cdot 10^{14}$ cm^{-3} and $2 \cdot 10^{13}$ cm^{-3} for the 2 and 200 Ω·cm material, respectively. However because of higher noise at lower injection level, $\Delta n = 5 \cdot 10^{14}$ cm^{-3} is chosen for ΔN_{leq} calculation (if not stated otherwise) as a trade-off between neglecting the influence of FeB-pair dissociation and minimizing noise. This in turn means for the 200 Ω·cm material that a possible BRD might be underestimated in ΔN_{leq} and thus in $\Delta N_{\text{leq},b}$ if the samples are affected by FeB-pair dissociation. In the context of this experiment, the state of possible FeB pairs would differ between the reference point and all other points because of the treatment conditions (100 °C, 800 W/m^2). A possible Fe concentration (not measured here) would therefore only influence the absolute values of ΔN_{leq} and not the kinetics. For the J_{0s} analysis, the range of Δn is varied from sample to sample in the range of $0.5-1.5 \cdot 10^{16}$ cm^{-3}.

IV. Results

A. Overview of Base Material and SiN$_x$:H Deposition Variation

As can be seen in Fig. 3, varying base material and SiN$_x$:H deposition leads to different behavior under the given treatment conditions in the climate chamber.

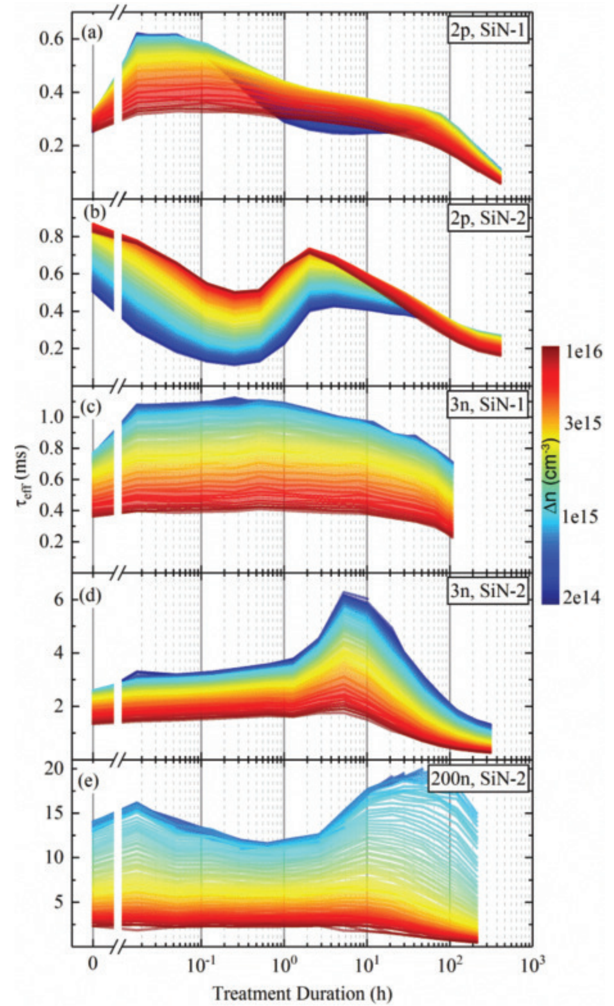

Fig. 3. Effective lifetime over treatment duration for five samples from Group II with different base materials and SiN$_x$:H layers from different deposition tools, as shown in each graph separately. The colors represent τ_{eff} at different injection levels (scale bar) from transient measurements. Note the different scaling of the lifetime axes. (For interpretation of the references to color in the figures, the reader is referred to the web version of this article.)

Whereas Fig. 3(a) and (b) shows a LeTID behavior rather common in FZ-Si [8], [9], [11] as schematically depicted in Fig. 1, they differ in their LeTID kinetics with respect to the minima of BRD. Fig. 3(c) depicts a τ_{eff} behavior already seen for n-type samples not being affected by bulk degradation and regeneration, but by SRD [5], [9]. The n-type sample shown in Fig. 3(d) featuring a differently deposited SiN$_x$:H compared with Fig. 3(c) shows an increase in τ_{eff} without significant preceding BRD. In Fig. 3(e), a 200 Ω·cm n-type sample is shown, which features a decrease and following increase in τ_{eff} at low injection levels similar to p-type samples, but on a significantly higher lifetime level.

In addition, samples with SiN-1 show a strong increase of τ_{eff} mainly at lower injection levels in the first two data points. This increase is primarily not because of the dissociation of FeB pairs, which can be seen from the injection dependent behavior of τ_{eff} not resulting in a crossover point [21] [deep blue curves in Fig. 3(a) and (c)]. This increase can be attributed to an effect called "light induced curing" [22], which appears

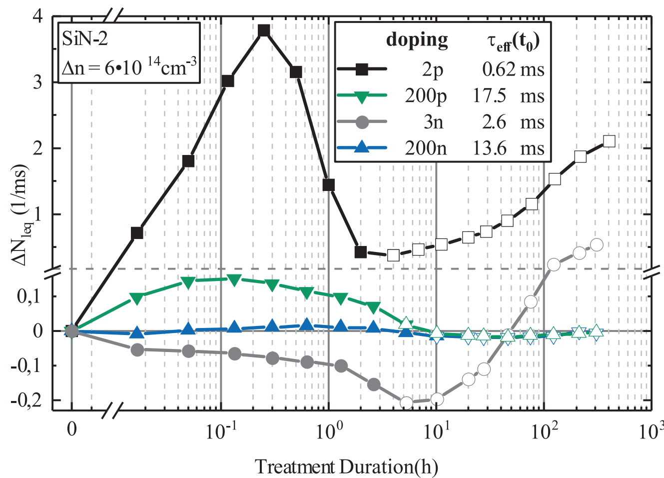

Fig. 4. Lifetime-equivalent defect density during treatment of four samples with different base material. As reference point, τ_{eff} before treatment was used and ΔN_{leq} was evaluated at $\Delta n = 6 \cdot 10^{14}$ cm^{-3}. The black, gray, and blue curve belong to the same sample as graphs (b), (d), and (e) from Fig. 3. Open symbols represent data points influenced by SRD.

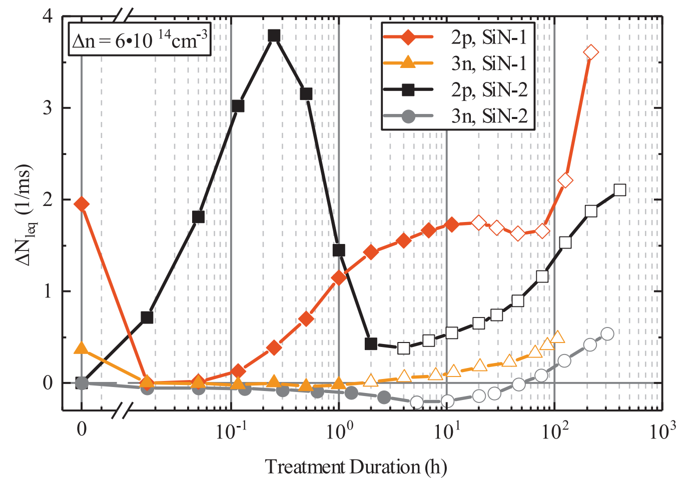

Fig. 5. Lifetime-equivalent defect density during treatment of samples with different doping type and SiN$_x$:H deposition. As reference point, τ_{eff} before treatment was used and ΔN_{leq} was evaluated at $\Delta n = 6 \cdot 10^{14}$ cm^{-3}. Reference point for samples with SiN-1 is the first τ_{eff} value after start of treatment and for samples with SiN-2 τ_{eff} before treatment. Open symbols represent data points influenced by SRD. The data belong to the same samples as the data in Fig. 3(a)–(d).

on fired samples with this specific SiN-1 layer. The exact cause for this increase is not yet known, although its cause might be linked to hydrogen [22]. Whether the smaller increase in n-type samples with SiN-2 [compare Fig. 3(d) and (e)] is because of a similar effect or not is beyond the scope of this article.

All samples in Fig. 3 show a decrease of τ_{eff} at higher injections (red curves) at later treatment times leading to a drop of τ_{eff} values in every injection level. This is the result of SRD, which can be described by, e.g., increasing J_{0s} values [8] or, in this article, by $\Delta N_{\text{leq},s}$ [see (2)]. In addition, the behavior of SRD seems to depend on the type of SiN$_x$:H layer.

B. Influence of Base Material

To have a closer look at the influence of the base material, four fired samples from Group II with different doping type and base doping are investigated. Fig. 4 shows the ΔN_{leq} values of these samples with open symbols indicating data points under the influence of an increased surface recombination and therefore an increasing $\Delta N_{\text{leq},s}$. The black curve depicts one LeTID cycle quite well: BRD leads to increasing bulk recombination rate and therefore increasing ΔN_{leq}, whereas the subsequent regeneration leads to a reduced recombination rate in the bulk. SRD starts to influence τ_{eff} at around 4 h, resulting in increasing $\Delta N_{\text{leq},s}$ and therefore ΔN_{leq} values (denoted by open symbols).

It can be seen that both p-type samples are affected by BRD, although the 2p sample (black) does display higher ΔN_{eq} values. This is because of using $\Delta n = 6 \cdot 10^{14}$ cm^{-3} for every sample regardless of the base doping N_d. Whereas for the 2p sample $\Delta n \approx 0.1 \cdot N_d$, the 200p sample is evaluated at $\Delta n \approx 10 \cdot N_d$. Assuming a deep defect, the 200p sample is underestimated by nearly an order of magnitude (see, e.g., [16]). The same argument holds true for the 200n sample (blue) whose ΔN_{leq} values are quite small while the τ_{eff} changes are clearly visible in Fig. 3(e). Whereas the 3n sample does not show any degradation in accordance with [5] and [9], a decrease of ΔN_{leq} is visible for the 200n sample. Recent results have shown that LeTID in n-type mc-Si can occur [23], [24], whereas these results indicate that LeTID also might influence 200 Ω·cm n-type FZ-Si.

As can be seen in Fig. 3(d), the rise of τ_{eff} at around 6 h is mostly at low injections, therefore probably linked to a bulk effect. This could lead to the conclusion that both the increase in n-type and regeneration in p-type come from the same effect. Assuming this, the active defect should already exist in the n-type sample after firing and before treatment in the climate chamber. Another possible explanation could be that this increase of τ_{eff} is a light-induced phenomenon linked to fired samples with this specific SiN-2 for 3n samples with SiN-1 samples not showing the increase [compare Fig. 3(c)]. On the other hand, the 200n sample in Fig. 4 shows first an increase and a subsequent decrease of ΔN_{leq}. It is possible that this is caused by the same defect structure responsible for BRD possibly being an addition to recent findings of LeTID in n-type mc-Si [25].

C. Different SiN$_x$:H Layer Deposition Tools

In Fig. 5, samples with SiN$_x$:H layers from two different tools are compared. Both displayed n-type samples with different SiN$_x$:H type do not show bulk degradation. Whereas the sample with SiN-1 (yellow) does not show any changes in bulk recombination, the sample with SiN-2 (gray) shows a decrease in bulk recombination with a minimum recombination rate at around 6 h, which is already discussed before. In addition, the other n-type sample with SiN-1 [orange curve in Fig. 5 or Fig. 3(c)] does not show signs of a decreased recombination rate. In addition, both n-type samples show surface degradation.

The p-type samples with different SiN$_x$:H types differ from each other in their respective kinetics. The sample with SiN-1 (red) shows a lower maximum of ΔN_{leq}, which appears at a

much later treatment time compared with the sample with SiN-2 (black). While the black curve displays three clear phases with bulk degradation, bulk regeneration, and surface degradation, the red curve does not show any bulk regeneration, although one would expect the red curve to drop after a maximum at around 10 h due to bulk regeneration. The onset of surface degradation (depicted as open symbols) leads to increased recombination at this point in time. Because of this, the regeneration effect is only slightly visible in τ_{eff} and therefore ΔN_{leq}, which leads to the plateau-like behavior of ΔN_{leq}.

Recent results on mc-Si [26], [27] have shown a correlation of defect density with increasing H release from the SiN_x:H layer. In accordance with these results, the lower maximum in ΔN_{leq} of the red curve suggests that less hydrogen was released into the bulk. This correlates to FTIR measurements (not displayed here) that show a larger density of N–H bonds, which may indicate a larger H density in SiN-2. The maximum of ΔN_{leq} is also influenced by the H out-diffusion rates of both SiN_x:H layers. Thus, as pointed out in a recent publication [28], bulk H density measurements are necessary to confirm the impact of SiN_x:H layer properties on LeTID kinetics, which are beyond the scope of this article.

In addition, the maximum is visible at a later treatment time probably because of the transition rates k_{AB} and k_{BC} of the sample with SiN-1 being lower. Different rate constants could as well reduce the maximum of ΔN_{leq} compared with the 2p sample with SiN-2. Both effects, lower and later maximum because of different rate constants and possibly different hydrogen density in the SiN_x:H layer, are probably because of different SiN_x:H deposition conditions and their respective influence since it is the only difference in both samples' treatment.

D. *Influence of Different Temperature Steps on BRD*

In the next step, 2p samples with SiN-1 (Group I) are taken and subjected to a variation of temperature steps. In order to investigate their influence on the bulk phenomena, $\Delta N_{\text{leq},b}$ is calculated by subtracting surface-related effects [see (3)].

The sample without temperature treatment ("As-deposited," black curve) in Fig. 6 shows BRD and regeneration contradicting results in mc-Si that imply the necessity of a firing step in order to evoke LeTID [13]. This suggests that defect precursors (state A) must be present after this specific SiN-1 deposition. Whether the precursors already exist before deposition or the deposition itself leads to the formation of precursors is not yet clear. A similar result in FZ-Si was already presented in [15]. A firing step (blue curve) changes the kinetics in comparison to the As-deposited sample. The maximum of $\Delta N_{\text{leq},b}$ is higher and is reached at a later treatment time. One possible explanation for the higher maximum could be the diffusion of H from the SiN_x:H layer into the bulk during the firing step (see, e.g., [29]). This might lead to an increase in precursor defect density resulting in an increased N_B and therefore $\Delta N_{\text{leq},b}$. Another possibility could be that the firing step alters the transition rates, leading to the larger maximum. As an addition, the firing step must have reduced k_{AB} and/or k_{BC} for the maximum appears at a later treatment time.

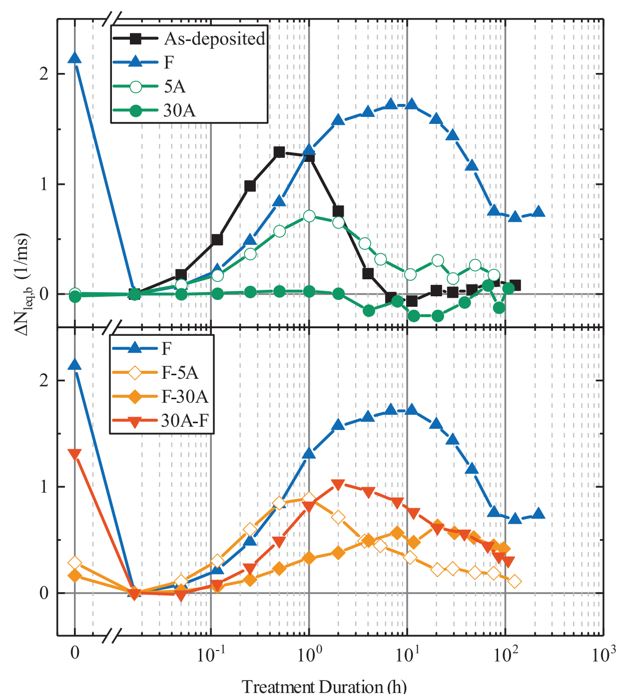

Fig. 6. Influence of different temperature steps on the lifetime-equivalent defect density of the bulk over treatment duration. Investigated samples are 2 Ω·cm p-type with SiN-1 from Group I. F—fired, 5/30A—annealed for 5/30 min, F-5A—fired and annealed for 5 min, etc. Reference point is the first τ_{eff} value after treatment start.

By only annealing a sample, the impact of LeTID can be reduced as seen by the green curves in Fig. 6. The sample with a 5-min annealing step shows BRD and regeneration but with a lower maximum compared with the As-deposited sample. Annealing for 30 min leads to a sample without a visible BRD and therefore without any relevant changes in $\Delta N_{\text{leq},b}$. A possible reason for the behavior of both annealed samples is that the annealing step reduces the precursor density. It is known that LeTID also occurs in the dark [30]. With the annealing taking place at 450 °C without additional illumination, it is possible that the precursor defect density is being reduced by being transitioned into the regenerated state C. Since the 5A curve in Fig. 6 shows BRD, the depletion of defect precursors (state A) is probably linked to annealing time. From recent studies investigating the impact of dark annealing in mc-Si [31], [32], it can be concluded that a higher annealing temperature leads to a faster regeneration and therefore a faster transition from states A to C. For temperatures above 275 °C, no clear degradation is observed during dark anneal [31], which could be because of high transition rates k_{AB} and k_{BC} as a result of higher annealing temperature. This could indicate that at 450 °C, BRD and regeneration are happening. The time of dark anneal would therefore be the factor determining what part of the precursor density is already regenerated into state C. Although with such high transition rates no BRD is visible in τ_{eff} making a direct insight into the mechanism of dark annealing at 450 °C difficult without knowing and measuring the species related to the specific states A and C.

This theory is at first glance in contradiction to results from Herguth *et al.* [33], [34] who investigated LeTID kinetics in (fired) mc-Si solar cells at high temperatures combined with illumination above 1 sun. They showed that at temperatures above 300 °C, no LeTID is visible anymore but subsequent treatments at 121 °C do again show LeTID [34]. This in turn indicates that at these high temperatures, the samples are not "cured" from LeTID, or at least not enough active defects are transitioned to the regenerated state C. With this result, one would expect the 30 A sample to degrade too. Since the 30 A sample does not show any BRD, the differences between both experiments and their respective influence on the kinetics are quite interesting. One possible aspect—a firing step before annealing—is investigated further in the following.

In addition, it appears that the annealing step itself alters k_{AB} and k_{BC} of the 5A sample with the maximum being slightly later. This could in principle as well be the explanation for the lower maximum, which would mean that in the 30A case, the rates are altered such that no visible defect density ΔN_B exists.

If a sample is first annealed for 30 min and then fired (red curve in Fig. 6), a maximum is once again observed but being lower compared with the fired sample (blue curve). As previously explained, the annealing step nearly depletes the precursor defect density. A subsequent firing step presumably leads to diffusion of H from the SiN_x:H layer into the bulk and therefore to an increase in precursor density, which leads to a visibly maximum compared with the sample with 30 min annealing (green, closed symbols) but with a lower maximum compared with the fired sample (blue curve).

Firing a sample and annealing it afterward leads yet again to different kinetics (orange curves). As expected from previous samples, the subsequent annealing step lowers the maximum of $\Delta N_{\mathrm{leq},b}$ compared with the fired sample because of the said reasons. Although now the main difference between 5 and 30 min annealing is not only the height of the maximum but also the treatment time at which the maximum occurs. Whereas 5 min annealing after firing leads to a maximum at around 1 h, the 30 min annealing results in a maximum at around 20 h. Therefore, the annealing step in itself alters the kinetics, but also its duration has an effect. Similar results regarding different kinetics with different annealing steps have been found in mc-Si [32], [35]. Although in these publications, the annealing temperature was varied instead of the annealing time. A similar trend was found with lower annealing temperatures leading to an earlier maximum of defect density, whereas higher annealing temperatures lead to a later maximum. One could argue that lower annealing temperatures have similar effects as lower annealing times on the BRD kinetics. A possible reason for this behavior is that this bulk degradation is associated with a movement of defects or one defect species (e.g., hydrogen) [32]. The annealing step might modify the defect precursor distribution, which then has an influence on the degradation kinetics leading to k_{AB} and k_{BC} varying between different annealing durations.

The results of the F-30A sample are in agreement with the investigations of Herguth *et al.* [33], [34] who found that treating fired mc-Si samples at 380 °C under illumination does not lead to stable samples under subsequent treatment at 121 °C and

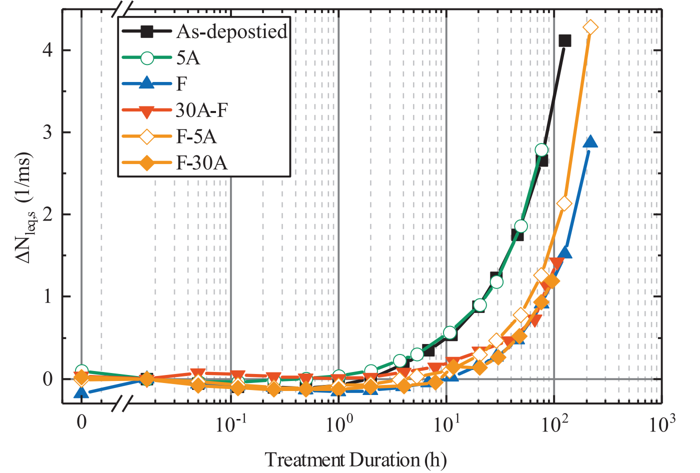

Fig. 7. Influence of different temperature steps on the lifetime-equivalent defect density of the surface over treatment duration, therefore on SRD. Investigated samples are 2 Ω·cm p-type with SiN-1 from Group I. F—fired, 5/30A—annealed for 5/30 min, F-5A—fired and annealed for 5 min, etc. Reference point is the first τ_{eff} value after treatment start.

illumination. This in turn means that the F-30A sample reacts differently to the annealing step compared with the 30A sample. While the annealing step leads to a stable sample regarding BRD, an additional firing step influences the sample such that defect precursors (state A) still exist in a noticeable amount after this specific annealing. Samples F-30A and 30A indicate that the firing step seems to be the key to having a stable or nonstable sample after annealing. In another recent study [36], fired mc-Si samples that were annealed for 18.5 h at 300 °C showed nearly no bulk degradation. This suggests that the underlying mechanism to deactivate LeTID in the 30A sample and the effect seen in samples from [36] could be the same with the firing step slowing down the process in such a way that much longer annealing times are needed. Although additional investigations are needed to specifically investigate why the firing step has such an influence and if there are differences between mc-Si and FZ-Si regarding the influence of different annealing conditions since most of the references cited here studied mc-Si. Combined with further studies with different combinations of firing and annealing step parameters this could lead to a more thorough understanding on how LeTID kinetics are influenced by these temperature steps and thus lead to more clues about the defect species and/or structure of LeTID.

E. Influence of Different Temperature Steps on SRD

SRD is investigated by first calculating J_{0s} and then $\Delta N_{\mathrm{leq},s}$ according to (2) from 2p samples with SiN-1 and different temperature steps. SRD in samples with SiN_x:H layers most likely originates from a degradation of the chemical passivation as shown by Sperber *et al.* [8]. By determining $\Delta N_{\mathrm{leq},s}$, one obtains information about the change of recombination active defects at the surface and therefore the kinetics of SRD. The samples in Fig. 7 form two groups in regard to their kinetics. The first group consists of an As-deposited sample and a sample with 5 min

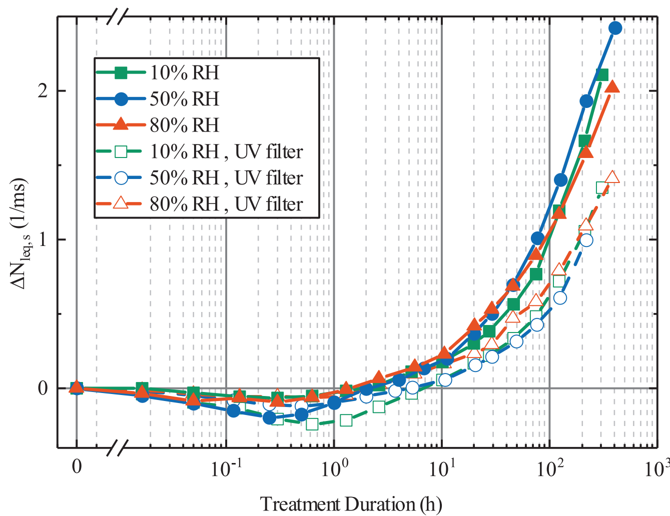

Fig. 8. Influence of different humidity and of samples under a UV filter during treatment on the lifetime-equivalent defect density of the surface, therefore on SRD. Investigated 2p samples with SiN-2 are from Group II, with reference point before treatment. Samples are investigated at 10%, 50%, and 80% RH. UV filter blocks photons up to 520 nm and approximately 40% of light intensity.

annealing. Compared with the other group—consisting of four samples having the firing step in common—the rise of $\Delta N_{\mathrm{leq},s}$ occurs at earlier treatment times. This means that it is probably not the annealing step that influences the SRD kinetics, but the firing step.

This could imply that the firing step influences the Si–SiO$_x$ interface responsible for chemical passivation and thus influences degradation kinetics by decreasing the transition rate k_{SRD}. In addition, it is assumed that H might play a role in SRD [8]. As the firing step is known to enhance diffusion of H [29], it might influence SRD kinetics by changing the spatial distribution or density of H. Hereby, only the influence of temperature steps on the transition rate k_{SRD} can be investigated. To examine their influence on the maximum defect density and on the transition rate of the regeneration, longer treatment durations are necessary.

F. *Influence of Humidity on SRD*

As the defect causing SRD is not yet fully understood, 2p fired samples with SiN-2 are investigated in order to determine the influence of humidity on SRD. As shown in Fig. 8, samples were treated at 10%, 50%, and 80% RH. In addition, a UV filter was used on some samples, which blocks photons up to 520 nm resulting in around 40% intensity loss, with the intention to investigate the influence of UV light on SRD.

The samples placed under a UV filter do show SRD, which indicates that UV light is not responsible for SRD. This is in accordance with [8] where it was demonstrated that the nonilluminated side also suffers from SRD, leading to the conclusion that SRD is a carrier-induced phenomenon. Although the samples under the UV filter show a slower degradation compared with the samples without a filter. Since a lower intensity leads to a lower temperature of around 5 °C, it is likely that either the reduced intensity or the temperature or both combined lead to a slower degradation.

The samples with and without a UV filter, respectively, do show a very similar behavior regardless of the set humidity of the climate chamber. This indicates that humidity as a possible factor causing SRD can be ruled out which is in accordance with results indicating that SiN$_x$:H protects the surface passivation against humidity [37], [38]. With this result, it is unlikely that humidity influences LeTID since it is a BRD phenomenon, although further investigations might be necessary to confirm this assumption.

V. Conclusion

As shown, LeTID kinetics in FZ-Si can be influenced by several factors. LeTID was found to occur in p-type 2 and 200 Ω·cm samples as well as weakly in 200 Ω·cm n-type, whereas 2 Ω·cm n-type samples did not show typical LeTID behavior. Different SiN$_x$:H deposition tools and different subsequent temperature steps lead to different BRD kinetics. The changes in the BRD kinetics can be seen in the transition rate k_{AB} and the maximum of $\Delta N_{\mathrm{leq},b}$, which is directly related to the change in density of the recombination active defects ΔN_B. The firing step leads to a larger maximum $\Delta N_{\mathrm{leq},b}$ value because of diffusion of H from the SiN$_x$:H layer into the Si bulk, although this effect might depend on the firing temperature as shown in [15]. The firing step changes either the defect precursor density or the transition rates such that the maximum of $\Delta N_{\mathrm{leq},b}$ increases. The annealing step on the other hand reduces presumably the precursor defect density although the underlying mechanism is not clear yet.

The influence of SiN$_x$:H deposition and subsequent temperature steps on degradation rate k_{AB} can best be described by assuming that BRD involves a movement of defects and/or defect precursors. The different temperature steps can vary the distribution of defect precursors and thus influence the movement in such a way that the degradation takes place faster or slower depending on the precursor distribution before treatment.

With respect to SRD kinetics, a difference between fired and nonfired samples has been observed, with fired samples showing a slower degradation rate. This may be due either to a change in the Si-SiO$_x$ interface or to a possibly different distribution of H. It has been shown that SRD is not affected by changing the humidity in the atmosphere. SRD also occurs without UV light, but is dependent on light intensity and temperature, probably because of being a carrier induced degradation phenomenon.

Thus, varying the initial sample state allows a specific and extensive investigation of LeTID using a wide range of parameters to accurately determine effects with negligible influence of secondary effects.

Acknowledgment

The authors would like to thank B. Rettenmaier and W. Franchini for technical support and F. Geml for help with sample preparation.

REFERENCES

[1] K. Ramspeck *et al.*, "Light induced degradation of rear passivated mc-Si solar cells," in *Proc. 27th Eur. PV Sol. Energy Conf. Exhib.*, 2012, pp. 861–865.

[2] D. Chen *et al.*, "Evidence of an identical firing-activated carrier-induced defect in monocrystalline and multicrystalline silicon," *Sol. Energy Mater. Sol. Cells*, vol. 172, pp. 293–300, 2017.

[3] F. Fertig *et al.*, "Mass production of p-type Cz silicon solar cells approaching average stable conversion efficiencies of 22%," *Energy Proc.*, vol. 124, pp. 338–345, 2017.

[4] D. Sperber, A. Heilemann, A. Herguth, and G. Hahn, "Temperature and light-induced changes in bulk and passivation quality of boron-doped float-zone silicon coated with SiN_x:H," *IEEE J. Photovolt.*, vol. 7, no. 2, pp. 463–470, Mar. 2017.

[5] T. Niewelt *et al.*, "Light-induced activation and deactivation of bulk defects in boron-doped float-zone silicon," *J. Appl. Phys.*, vol. 121, no. 18, May 14, 2017, Art. no. 185702.

[6] J. Lindroos and H. Savin, "Review of light-induced degradation in crystalline silicon solar cells," *Sol. Energy Mater. Sol. Cells*, vol. 147, pp. 115–126, Apr. 2016.

[7] F. Kersten *et al.*, "Degradation of multicrystalline silicon solar cells and modules after illumination at elevated temperature," *Sol. Energy Mater. Sol. Cells*, vol. 142, pp. 83–86, 2015.

[8] D. Sperber, A. Graf, D. Skorka, A. Herguth, and G. Hahn, "Degradation of surface passivation on crystalline silicon and its impact on light-induced degradation experiments," *IEEE J. Photovolt.*, vol. 7, no. 6, pp. 1627–1634, Nov. 2017.

[9] D. Sperber, A. Graf, A. Heilemann, A. Herguth, and G. Hahn, "Bulk and surface instabilities in boron doped float-zone samples during light induced degradation treatments," *Energy Proc.*, vol. 124, pp. 794–798, 2017.

[10] T. H. Fung *et al.*, "A four-state kinetic model for the carrier-induced degradation in multicrystalline silicon: Introducing the reservoir state," *Sol. Energy Mater. Sol. Cells*, vol. 184, pp. 48–56, Sep. 2018.

[11] D. Sperber, A. Schwarz, A. Herguth, and G. Hahn, "Enhanced stability of passivation quality on diffused silicon surfaces under light-induced degradation conditions," *Sol. Energy Mater. Sol. Cells*, vol. 188, pp. 112–118, 2018.

[12] T. Niewelt *et al.*, "Understanding the light-induced degradation at elevated temperatures: Similarities between multicrystalline and floatzone p-type silicon," *Prog. Photovolt., Res. Appl.*, vol. 26, no. 8, pp. 533–542, 2018.

[13] C. E. Chan *et al.*, "Rapid stabilization of high-performance multicrystalline p-type silicon PERC cells," *IEEE J. Photovolt.*, vol. 6, no. 6, pp. 1473–1479, Nov. 2016.

[14] D. Sperber, A. Herguth, and G. Hahn, "On improved passivation stability on highly-doped crystalline silicon and the long-term stability of regenerated Cz-Si," *Sol. Energy Mater. Sol. Cells*, vol. 185, pp. 277–282, Oct. 2018.

[15] D. Sperber, F. Furtwängler, A. Herguth, and G. Hahn, "Does LeTID occur in c-Si even without a firing step?" *AIP Conf. Proc.*, vol. 2147, no. 1, 2019, Art. no. 140011.

[16] A. Herguth, "On the lifetime-equivalent defect density: Properties, application, and pitfalls," *IEEE J. Photovolt.*, vol. 9, no. 5, pp. 1182–1194, Sep. 2019.

[17] A. Kimmerle, J. Greulich, and A. Wolf, "Carrier-diffusion corrected J_0-analysis of charge carrier lifetime measurements for increased consistency," *Sol. Energy Mater. Sol. Cells*, vol. 142, pp. 116–122, 2015.

[18] W. A. Lanford and M. J. Rand, "Hydrogen content of plasma-deposited silicon-nitride," *J. Electrochem. Soc.*, vol. 124, no. 8, pp. C286–C286, 1977.

[19] D. Sperber, A. Herguth, and G. Hahn, "Investigating possible causes of light induced degradation in boron-doped float-zone silicon," in *Proc. 33rd Eur. PV Sol. Energy Conf. Exhib.*, 2017, pp. 565–568.

[20] D. Sperber, "Bulk and surface related degradation phenomena in monocrystalline silicon at elevated temperature and illumination," Ph.D. dissertation, Fachbereich Physik, Universität Konstanz, Konstanz, Germany, 2019.

[21] D. H. Macdonald, L. J. Geerligs, and A. Azzizi, "Iron detection in crystalline silicon by carrier lifetime measurements for arbitrary injection and doping," *J. Appl. Phys.*, vol. 95, no. 3, pp. 1021–1028, 2004.

[22] S. Joos *et al.*, "Light induced curing (LIC) of passivation layers deposited on native silicon oxide," *Energy Proc.*, vol. 27, pp. 349–354, 2012.

[23] C. Vargas *et al.*, "Degradation and recovery of n-type multi-crystalline silicon under illuminated and dark annealing conditions at moderate temperatures," *IEEE J. Photovolt.*, vol. 9, no. 2, pp. 355–363, Mar. 2019.

[24] H. C. Sio *et al.*, "Light and elevated temperature induced degradation in p-type and n-type cast-grown multicrystalline and mono-like silicon," *Sol. Energy Mater. Sol. Cells*, vol. 182, pp. 98–104, Aug. 1, 2018.

[25] D. Chen *et al.*, "Hydrogen induced degradation: A possible mechanism for light- and elevated temperature-induced degradation in n-type silicon," *Sol. Energy Mater. Sol. Cells*, vol. 185, pp. 174–182, Oct. 2018.

[26] C. Vargas *et al.*, "Carrier-induced degradation in multicrystalline silicon: Dependence on the silicon nitride passivation layer and hydrogen released during firing," *IEEE J. Photovolt.*, vol. 8, no. 2, pp. 413–420, Mar. 2018.

[27] U. Varshney *et al.*, "Evaluating the impact of SiN_x thickness on lifetime degradation in silicon," *IEEE J. Photovolt.*, vol. 9, no. 3, pp. 601–607, May 2019.

[28] D. Bredemeier, D. C. Walter, R. Heller, and J. Schmidt, "Impact of hydrogen-rich silicon nitride material properties on light-induced lifetime degradation in multicrystalline silicon," *Phys. Status Solidi—Rapid Res. Lett.*, vol. 13, no. 8, Aug. 2019, Art. no. 1900201.

[29] S. Wilking, S. Ebert, A. Herguth, and G. Hahn, "Influence of hydrogen effusion from hydrogenated silicon nitride layers on the regeneration of boron-oxygen related defects in crystalline silicon," *J. Appl. Phys.*, vol. 114, no. 19, 2013, Art. no. 194512.

[30] D. Sperber, A. Herguth, and G. Hahn, "Instability of dielectric surface passivation quality at elevated temperature and illumination," *Energy Proc.*, vol. 92, pp. 211–217, 2016.

[31] S. Y. Liu *et al.*, "Impact of dark annealing on the kinetics of light- and elevated-temperature-induced degradation," *IEEE J. Photovolt.*, vol. 8, no. 6, pp. 1494–1502, Nov. 2018.

[32] C. Chan *et al.*, "Modulation of carrier-induced defect kinetics in multi-crystalline silicon PERC cells through dark annealing," *Sol. RRL*, vol. 1, no. 2, 2017, Art. no. 1600028.

[33] A. Herguth, C. Derricks, P. Keller, and B. Terheiden, "Recovery of LeTID by low intensity illumination: Reaction kinetics, completeness and threshold temperature," *Energy Proc.*, vol. 124, pp. 740–744, 2017.

[34] A. Herguth, P. Keller, and N. Mundhaas, "Influence of temperature on light induced phenomena in multicrystalline silicon," *AIP Conf. Proc.*, vol. 1999, 2018, Art. no. 130007.

[35] C. E. Chan *et al.*, "Investigation of carrier-induced defect behavior in p-type multicrystalline silicon," in *Proc. 44th IEEE Photovolt. Spec. Conf.*, 2017, pp. 2576–2581.

[36] M. Yli-Koski, M. Serue, C. Modanese, H. Vahlman, and H. Savin, "Low-temperature dark anneal as pre-treatment for LeTID in multicrystalline silicon," *Sol. Energy Mater. Sol. Cells*, vol. 192, pp. 134–139, Apr. 2019.

[37] X. Dai and K. R. McIntosh, "Protection of Si-SiO_2 interfaces from damp heat by overlaying SiN_x and Si_3N_4 coatings," in *Proc. 35th IEEE Photovolt. Spec. Conf.*, 2010, pp. 3205–3209.

[38] W. S. Liang, D. Suh, J. Yu, J. Bullock, and K. J. Weber, "Degradation of the surface passivation of plasma-assisted ALD Al_2O_3 under damp-heat exposure," *Phys. Status Solidi (a)*, vol. 212, no. 2, pp. 274–281, Feb. 2015.

Benjamin Hammann received the master's degree in physics from the University of Konstanz, Konstanz, Germany, in 2019.

During his master's thesis with the Photovoltaic Division, he worked on degradation phenomena and in particular on LeTID in float-zone silicon.

Josh Engelhardt received his doctorate in physics from the University of Konstanz, Konstanz, Germany, in 2019.

Since 2015, he has been the Head of the industrial solar cell group as well as the process technology and safety group. His research of novel solar cell technologies and applications aims to advance regenerative energy source development.

David Sperber, photograph and biography not available at the time of publication.

Axel Herguth received the Diploma degree in physics from the University of Konstanz, Konstanz, Germany, in 2006.

Since 2007, he has been the Head of the characterization group with the Photovoltaics Division, University of Konstanz. His research interests include the kinetics of defects in silicon in general, especially, the kinetic of the boron-oxygen-related defect, as well as characterization techniques for silicon wafers and solar cells.

Mr. Herguth received the Junior Einstein Award from SolarWorld in 2006 for his work on the avoidance of the boron-oxygen-related degradation.

Giso Hahn received the Ph.D. degree in physics from the University of Konstanz, Konstanz, Germany, in 1999.

Since 2009, he has been a Professor with the Department of Physics, University of Konstanz, where he is currently the Head of the Photovoltaics Division, which is focused on crystalline silicon materials and solar cell process development. His research interests include the characterization of promising low-cost materials for photovoltaic applications and the development of adapted solar cell processes for these and other materials.

Dr. Hahn is a member of the scientific committees of various conference series and workshops. Among other scientific and technological achievements, his group is interested in transferring technologies from the laboratory stage to the industry.